Article

Not peer-reviewed version

The Gárdos Channel and Piezo1 Revisited: Comparison between Reticulocytes and Mature Red Blood Cells

Polina Petkova-Kirova †, Nicoletta Murciano †, Julia Jansen †, Greta Simionato †, Giulia Iacono †, Maria Giustina Rotordam, Thomas John, Min Qiao, Laura Hertz, Arjan J. Hoogendijk, Nadine Becker, Christian Wagner, Marieke von Lindern, Stephane Egee, Emile Van den Akker, Lars Kaestner *

Posted Date: 17 October 2023

doi: 10.20944/preprints202310.1044.v1

Keywords: erythrocytes; reticulocytes; patch-clamp; membrane potential; NS309; Yoda1; TRAM34; calcium

Article

The Gárdos Channel and Piezo1 Revisited: Comparison between Reticulocytes and Mature Red Blood Cells

Polina Petkova-Kirova [1,2,+], Nicoletta Murciano [3,4,+], Julia Jansen [4,5,+], Greta Simionato [5,6+], Giulia Iacono [7,8+], Maria Giustina Rotordam [3], Thomas John [5], Min Qiao [4,5], Laura Hertz [4,5], Arjan J. Hoogendijk [7,8], Nadine Becker [3], Christian Wagner [5,9], Marieke von Lindern [7,8], Stephane Egee [10,11], Emile van den Akker [7,8] and Lars Kaestner [4,5,*]

1 Bulgarian Academy of Sciences, Institute of Neurobiology, Sofia, Bulgaria; kirovaps@yahoo.com
2 Saarland University, Biochemistry, 66123 Saarbrücken, Germany
3 Nanion Technologies, Munich, Germany; Nicoletta.Murciano@nanion.de, Giustina.Rotordam@nanion.de, Nadine.Becker@nanion.de
4 Saarland University, Theoretical Medicine and Biosciences, Campus University Hospital, 66421 Homburg, Germany; julia.jansen26@gmx.de, laurahertz@gmx.de, lars_kaestner@me.com
5 Saarland University, Department of Experimental Physics, 66123 Saarbrücken, Germany; thomas.john@uni-saarland.de, min.qiao@uni-saarland.de, christian.wagner@uni-saarland.de
6 Saarland University, Department of Experimental Surgery, Campus University Hospital, 66421 Homburg, Germany; greta.simionato@uni-saarland.de
7 Sanquin Research, Department of Hematopoiesis, Amsterdam, The Netherlands; G.Iacono@sanquin.nl, A.Hoogendijk@sanquin.nl, m.vonlindern@sanquin.nl, e.vandenakker@sanquin.nl
8 Landsteiner Laboratory, Amsterdam UMC, University of Amsterdam, Amsterdam, The Netherlands
9 Physics and Materials Science Research Unit, University of Luxembourg, Luxembourg, Luxembourg
10 Sorbonne Université, CNRS, UMR8227 LBI2M, Station Biologique de Roscoff, France; egee@sb-roscoff.fr
11 Laboratory of Excellence GR-Ex, Paris, France
* Correspondence: lars_kaestner@me.com
† These authors contributed equally to the paper.

Abstract: (1) Background: The Gárdos channel (KCNN4) and Piezo1 are the best-known ion channels in the red blood cell (RBC) membrane. Nevertheless, the quantitative electrophysiological behavior of RBCs and its heterogeneity are still not completely understood.; (2) Methods: Here we use state-of-the-art biochemical methods to probe for the abundance of the channels in RBCs. Furthermore, we utilize automated patch-clamp, based on planar chips, to compare the activity of the two channels in reticulocytes and mature RBCs. Besides this characterization, we performed membrane potential measurements to demonstrate the effect of channel activity and interplay on the RBC properties.; (3) Results: Both, Gárdos channel and Piezo1, albeit their average copy number of activatable channels per cell is in the single digit range, can be detected by transcriptome analysis of reticulocytes. Proteomics analysis of RBCs could only detect Piezo1 but not the Gárdos channel. Furthermore, they can be reliably measured in the whole-cell configuration of the patch-clamp method. While for the Gárdos channel the activity is higher in reticulocytes compared to mature RBCs, for Piezo1 the tendency is the opposite. While the interplay between Piezo1 and Gárdos channel cannot be followed using the patch-clamp measurements, it could be proved based on membrane potential measurements in populations of intact RBCs.; (4) Conclusions: We discuss the Gárdos channel and Piezo1 abundance, interdependencies and interactions in the context of their proposed physiological and pathophysiological functions, which are the passing of small constrictions, e.g., in the spleen, and their active participation in blood clot formation and thrombosis.

Keywords: erythrocytes; reticulocytes; patch-clamp; membrane potential; NS309; Yoda1; TRAM34; calcium

 doi:10.20944/preprints202310.1044.v1

1. Introduction

Ion channels in red blood cells (RBCs) are a peculiar topic for two main reasons:

(i) For a long time it has not been quite clear if ion channels in RBCs do have a physiological function or are just relicts [1,2]. Although in the meantime there is no doubt about the contribution of ion channels to RBC flow properties, especially passing constrictions [3–5] or their active contribution to thrombus and clot formation [6,7], the rumor for channels being relicts persists.

(ii) The low copy number of ion channels in the RBC membrane along with functional ion channel measurements without knowing the ion channels' molecular identity [8,9] and the abundance of channels at or even below the detection limit of classical biochemical methods [10,11].

Here we present a further investigation of the Gárdos channel and Piezo1 because these are the best-known channels in RBCs in the sense that they are increasingly described to be involved in biophysical-biochemical coupled processes in RBC physiology and pathophysiology [12–14]. This, however, does not mean that we already know all their regulation and interplay properties in RBCs, which can be distinctly different from the ones in other cell types [15].

The Gárdos channel was the first channel discovered in (human) RBCs taking advantage of the patch-clamp method [16,17]. These measurements were based on previous reports of Ca^{2+}-induced K^+ loss in RBC suspensions [18,19]. Numerous reports of single-channel recordings followed the initial description of the channel [20–27]. Finally, the Gárdos channel was identified on the molecular level as KCNN4 (hSK4, $K_{Ca}3.1$, IK1) [28]. However, in the RBC community, the KCNN4 channel is still referred to as the Gárdos channel [9,29]. In recent years with the advent of next-generation sequencing, mutations in the Gárdos channel were discovered and associated with *Hereditary Xerocytosis* and more recently more specific *Gárdos Channelopathy*, e.g. [14,30–36]. The copy number of Gárdos channels per cell is believed to be rather low; (25% of the cells contain 11-55 copies and 75% of the cells 1-5 channels according to Grygorczyk *et al.* [21] and in average 2.6 channels per cell according to Wolff *et al.* [37]). On the other hand the Gárdos channel provides a significant and measurable effect (Ca^{2+}-induced K^+ loss).

The natural history of Piezo1 in RBCs was distinctly different compared to the Gárdos channel. Piezo1 and Piezo2 were identified as the molecular components of mechanosensitive ion channels in general [38,39]. Next, the identification of mutations of Piezo1 in patients suffering from *Hereditary Xerocytosis* proved the abundance of Piezo1 in RBCs [40–42]. There was a further functional/pharmacological (mainly based on the application of the agonist Yoda1 [43]) and molecular evidence for the abundance of Piezo1 in RBCs [44–48]. Interestingly, (similar to the Gárdos channel) it became evident that Piezo1 was recorded in RBCs even before its molecular identity was discovered [49,50].

Furthermore, transgenic animal models and microfluidic assays increased our understanding of the contribution of the interplay between the Gárdos channel and the mechanosensitive channel Piezo1 in volume adaptation required for RBCs to pass constrictions within the circulation [3–5]. In this context, we aimed to investigate the function and abundance of both, the Gárdos channel and Piezo1, in mature RBCs (erythrocytes) in comparison to reticulocytes and discuss their interaction and physiological function.

2. Results

2.1. Biochemical analysis

We performed a transcriptome analysis based on RNA isolated from reticulocytes. Figure 1A shows the outcome for the Gárdos channel and Piezo1 compared to VDAC2 [51] as a positive control. Please note the logarithmic scale in Figure 1A.

We also performed a proteomic analysis of RBCs. Figure 1B shows the mass spectrometry LFQ values Piezo1 is ranked 522 out of 752 detected proteins. Other ion channels including the Gárdos channel and VDAC2 could not be detected. The data present the average of four donors. Of note, other preparation methods of RBCs showed less consistent proteomic analysis results (data not shown). The challenges in the proteomic analysis in particular the strong dependence of the detection

Preprints (www.preprints.org) | NOT PEER-REVIEWED | Posted: 17 October 2023 doi:10.20944/preprints202310.1044.v1

results on the cell preparation mode, highlight a general challenge in RBC-related ion channel research [8].

To further illustrate this aspect, in the next step, we assessed cells with fluorescently labelled antibodies against the Gárdos channel and analyzed them in a flow cytometer. Figure 1C shows dot plots of staining for the transferrin receptor (CD71, pacific blue) *vs.* the Gárdos channel (KCNN4, FITC) for proerythroblasts (Figure 1Ca) and peripheral RBCs (Figure 1Cb). The comparison with the isotype reveals that the number of KCNN4 positive cells $(Q3+Q4)_{antibody}$-$(Q3+Q4)_{isotype}$ is with approximately 5% for proerythroblasts and 1% for erythrocytes is rather low. In summary, the abundance of the Gárdos channel is paltry and the method does not allow a reasonable quantification.

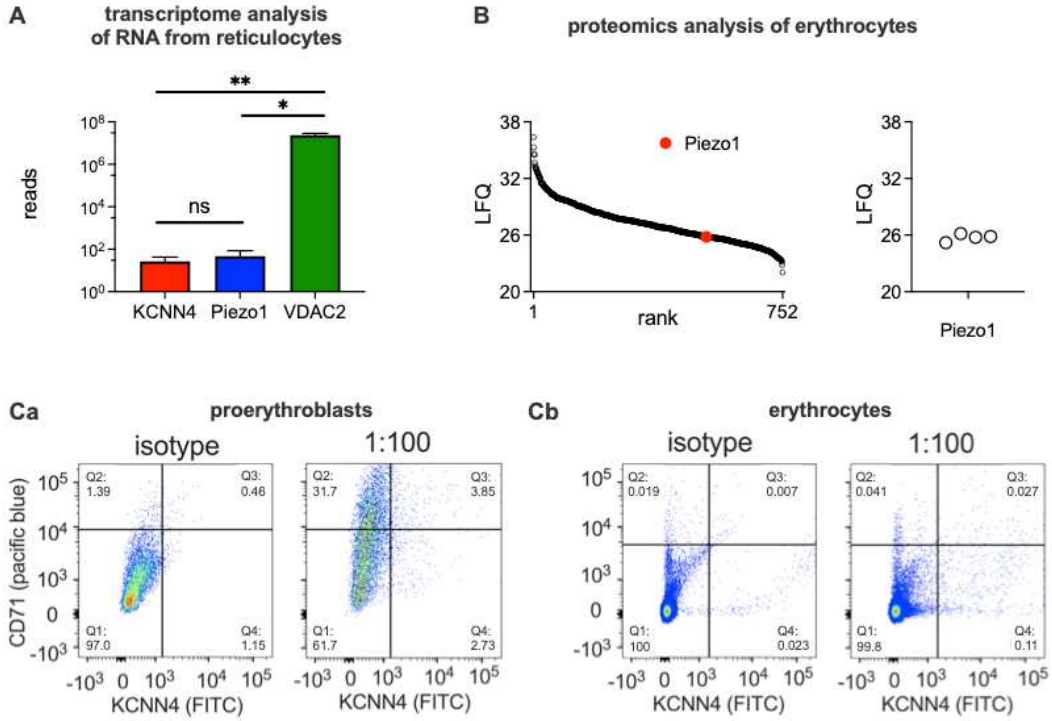

Figure 1. Transcriptome and protein analysis. Panel A shows the transcriptomic analysis for the Gárdos channel (KCNN4), Piezo1 and VDAC2 based in RNA isolated from circulating reticulocytes. The columns present the mean values from 4 donors with the error bars being SEM. Gárdos channel (KCNN4) is slightly lower in the reads compared to Piezo1 but the difference is not significant whereas both of them are significantly smaller than VDAC2. Comparisons of the means were tested depicting a $p>0.05$ for not significant (ns), * for $p<0.05$ and ** for $p< 0.01$. Panel B shows the result of the proteomic analysis performed on erythrocyte lysates from 4 different donors. Left diagram: LFQ values of all the proteins detected, the red dot indicates Piezo1. Right Diagram: Piezo1 LFQ values for the individual erythrocyte samples. The Gárdos channel (KCNN4) as well as VDAC2 were below the detection limit. Panel Ca shows a dot plot of Gárdos channel antibody (KCNN4, FITC) vs. transferrin receptor (CD71, pacific blue) for proerythroblasts presenting a 'positive control' for the isotype *vs.* antibody stains. Panel Cb shows the same measurements (but different gain settings) for red blood cells presenting the reticulocytes in sectors Q2 and Q3.

2.2. Patch-clamp analysis

The patch-clamp technique is the most direct approach to measure ion channels function as it directly measures the electrical current carried by ions passing the pore of the channel of interest. To ensure specificity of the measured current (channel) (or it could be said also to differentiate the current of interest) internal and external solutions of specific composition, particular voltage protocols and additional chemical or physical stimulation, were applied.

We based our measurements on previously reported protocols used for Piezo1 and the Gárdos channel [33,48] with slight modifications. The nature of the Gárdos channel and Piezo1 is vastly different and therefore necessitated different voltage protocols, which are outlined in Figure 2.

Preprints (www.preprints.org) | NOT PEER-REVIEWED | Posted: 17 October 2023 doi:10.20944/preprints202310.1044.v1

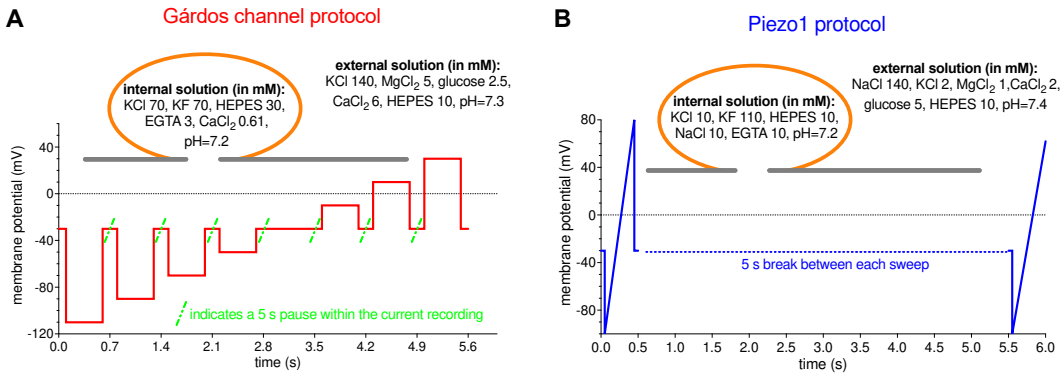

Figure 2. Patch-clamp measurement voltage protocols – a conceptual approach. Panel A shows the 'voltage step protocol' as applied for the Gárdos channel measurements. In panel B the 'ramp protocol' as used for Piezo1 recordings is shown. The inserts in both panels depict the contents of the internal and external solutions used for the measurements.

A "voltage-step" protocol was used to measure the Gárdos channel and a "ramp" protocol-to measure Piezo1. Ramps have the advantage of generating current-voltage relations directly and very rapidly and are especially suitable for studying rapidly activating currents. Step protocols measure the steady state current at a given voltage and depending on the duration of the step allow to analyze the kinetics of the current at each voltage and phenomena such as inactivation and desensitization. Due to the small number and single channel conductance of the Gárdos channels in RBCs [21,37], additional to its evaluation by considering the mean current at a certain voltage, an equally accurate assessment of the channel is given by analysis of the kinetics of the current [33]. A macroscopic whole-cell current, being the result of the summation of many smaller unit currents flowing through single ion channels, exhibits fluctuations about its mean level and those fluctuations are especially obvious when the Gárdos channel is activated by NS309. Thus a step protocol was considered for recording Gárdos channel currents (Figure 2A), in contrast to Piezo1, which is a fast inactivating channel (although less fast when activated with Yoda1) and a 'ramp protocol' was the more appropriate choice (Figure 2B).

Figure 3 shows Gárdos channel currents elicited by the voltage step protocol as outlined in Figure 2A for reticulocytes and mature RBCs. The pharmacological approach involved measuring the background current before applying a compound (Figure 3A, left traces), stimulating the Gárdos channel by application of NS309 (Figure 3A, middle traces) and as a last step blocking the Gárdos channel by application of its inhibitor TRAM34 (Figure 3A, right traces). As a Gardos current is considered the difference in currents before and after application of NS309, i.e., the current before application of NS309 being subtracted from the current after application of NS309, resulting current-voltage curves are given in Figure 3B. Although it is known that the Gárdos channel has not a linear conductance, in the measured voltage range between -110 mV and +30 mV, a linear regression gives a good approximation of the whole-cell conductances of the channel and these conductances (slopes in the diagram) were significantly different ($p=0.01$) between reticulocytes (G = 122 pS) and mature RBCs (G = 55 pS). The percentage of responding cells is provided in the pie charts (Figure 3C) revealing a slightly higher percentage of responding cells in the reticulocyte population compared to the one of mature RBCs.

Preprints (www.preprints.org) | NOT PEER-REVIEWED | Posted: 17 October 2023 doi:10.20944/preprints202310.1044.v1

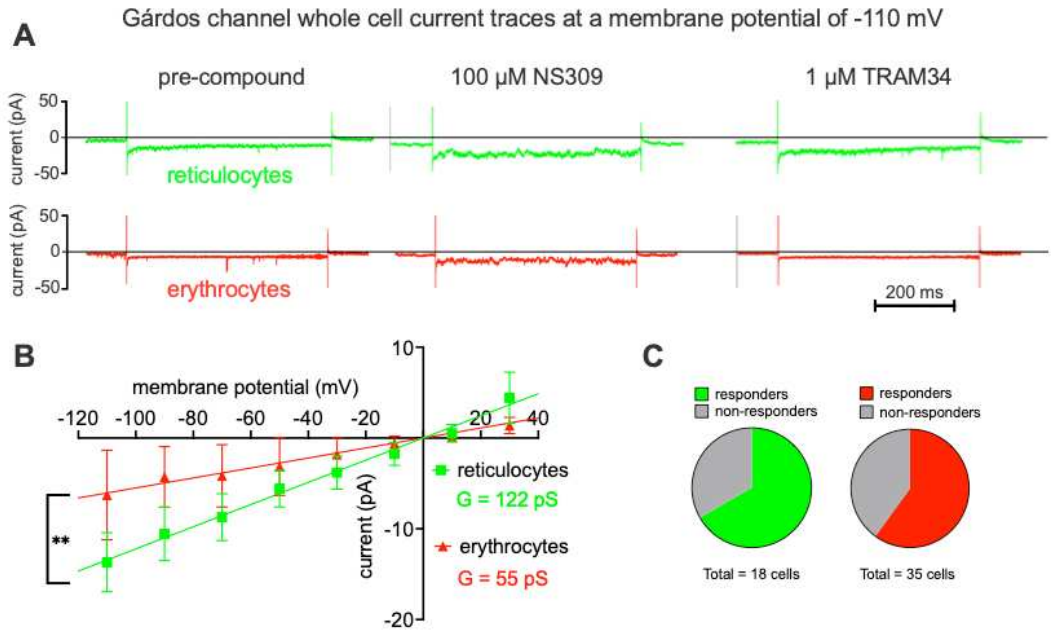

Figure 3. Gárdos channel measurements. Panel A shows representative raw current traces. The first 100 ms of each trace the voltage is clamped to -30 mV, followed by half a second clamped to -110 mV and then another 100 ms at -30 mV (compare Figure 2A). Green traces refer to reticulocytes and red traces to mature erythrocytes. The left traces are recordings before NS309 application, the middle traces depict channel activity after stimulation with 100 µM NS309, a specific Gárdos channel activator and finally the right traces show the response after application of the Gárdos channel blocker TRAM34 (1 µM). Panel B provides the current-voltage diagram for reticulocytes (n=13) and mature erythrocytes (n=10). Plotted are values of the difference in the mean current with and without NS309 as a read-out of the Gárdos current with error bars representing the standard error of the mean (SEM). Although the Gárdos channel is an inward rectifying channel, in the probed voltage range between -110 mV and 30 mV a linear fit well represents the whole-cell conductance which is 122 pS and 55 pS for reticulocytes and erythrocytes, respectively. The test of significant differences refers to the difference in the slope (conductance). ** indicates a p-value below 0.01. Panel C depicts pie charts indicating the percentage of responding and non-responding cells for reticulocytes (green) and mature red blood cells (red).

Figure 4 shows Piezo1 measurements applying the voltage ramp protocol as outlined in Figure 2B. The pharmacological concept was to measure the background current before applying a compound (Figure 4A, light green and orange traces for reticulocytes and mature RBCs, respectively). This was followed by stimulation of Piezo1 by application of Yoda1 (Figure 4A, green and red traces for reticulocytes and mature RBCs, respectively) and finally blocking Piezo1 (and putative other non-selective cation channels) by application of the unspecific inhibitor $GdCl_3$ (Figure 4A, dark green and dark red traces for reticulocytes and mature RBCs, respectively). Since activation of Piezo1 results in Ca^{2+}-influx, this Ca^{2+} could activate the Gárdos channel - so the recordings presented in Figure 4A could be the superposition of Piezo1 and Gárdos channel currents. To this end and to exclude the participation of the Gárdos channel currents the same experiments were repeated in the presence of the Gárdos channel inhibitor TRAM34 while stimulating the cells with Yoda1 (Figure 4B, same color code as Figure 4A).

Preprints (www.preprints.org) | NOT PEER-REVIEWED | Posted: 17 October 2023 doi:10.20944/preprints202310.1044.v1

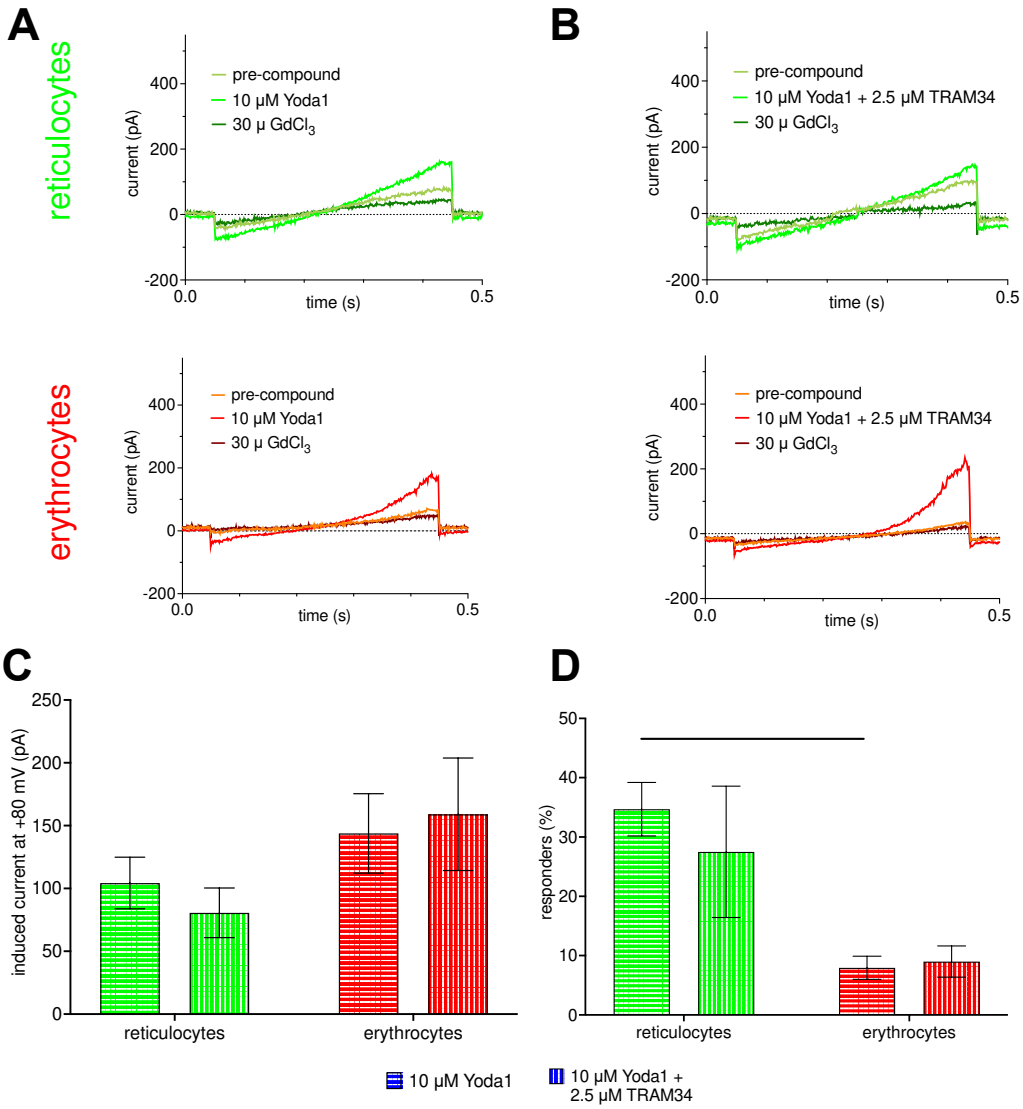

Figure 4. Piezo1 measurements. Panel A shows representative current traces. The first 50 ms of each trace the voltage is clamped to -30 mV, followed by a 400 ms ramp from -100 mV to 80 mV and then another 50 ms at -30 mV (compare Figure 3B). Green traces refer to cultured reticulocytes and red traces to mature erythrocytes. The recordings show traces before and after stimulation with 10 µM Yoda1, a specific Gárdos channel activator and after blockage with 30 µM $GdCl_2$. Panel B shows representative current traces in similarity to panel A, but the stimulation with 10 µM Yoda1 is accompanied by simultaneous inhibition of the Gárdos channel with 2.5 µM TRAM34. Panel C provides the bar graphs of the Yoda1-induced current for reticulocytes (n=21) and mature erythrocytes (n=20). Plotted are mean values with error bars representing the standard error of mean (SEM). Panel D depicts the percentage of responding cells per experiment for reticulocytes (green) and mature red blood cells (red). The test of significance was performed with an ordinary one-way ANOVA with Tukey's multiple comparisons test. ** refer to a p-value below 0.01.

Statistical analysis of the current ramps for the voltage of +80 mV is provided in a column diagram (Figure 4C). Albeit mature RBCs have a smaller surface area compared to reticulocytes the induced current is bigger for mature RBCs compared to reticulocytes in both experimental conditions (although not significant). The corresponding percentage of responding cells is also given in a column diagram (Figure 4D). The percentage of responding mature RBCs is on average below 10% and approximately one-third compared to reticulocytes.

2.3. Membrane potential measurements

Preprints (www.preprints.org) | NOT PEER-REVIEWED | Posted: 17 October 2023 doi:10.20944/preprints202310.1044.v1

The electrophysiological characterization of ion channels, as presented in Figures 3 and 4, is in fact rather a description of the biophysical properties of the channels, which should be related to function under physiological conditions. To this end, we present drug-induced membrane potential changes, which can successfully indicate channel interactions (in contrast to patch-clamp measurements) for intact RBCs.

To interpret the pharmacological stimulations, Figure 5 presents a step-by-step argumentation chain: Panel 5A shows the effect of an increase in the RBC K^+ permeability. The resting membrane potential of RBCs is approximately -12 mV. The addition of NS3623 blocks the RBC Cl^- conductance (which determines the resting potential), which results in a shift of the membrane potential towards 0 mV (equilibrium). Valinomycine acts as a K^+ pore and therefore the membrane potential after the addition of valinomycine could be calculated based on the K^+ distribution using the Nernst equation:

$$V = -\frac{RT}{zF} \times \ln \frac{[K^+]_{in}}{[K^+]_{out}} \quad (1)$$

where R is the universal gas constant, T is the temperature (in Kelvin, here 310 K), z is the ionic charge number ($z = 1$ for K^+) and F is the Faraday constant, amounting the first term to a constant of 26.7 mV. $[K^+]_{in}$ can be taken from the literature [52] to be 102 mM and $[K^+]_{out}$ from the experimental conditions (cp. legend of Figure 5A) as 9.9 mM. Thus the membrane potential calculates to -62.3 mV. This is in good agreement with the measured -64.2 mV hyperpolarization reached in the measurements. The addition of TritonX-100 is a calibration procedure for the membrane potential of 0 mV.

In Figure 5B it was tested if cellular hyperpolarization is also reached by activation of the Gárdos channel (Ca^{2+}-activated K^+ channel) by NS309. This is indeed the case, however, the polarization is a bit less pronounced for 3 reasons: (i) the K^+ concentration in the external solution is slightly different than in the experiments presented in panel A (compare figure legend); (ii) to assess the physiological effect of the Gárdos channel activation, no additional NS3623 to bloch the Cl^--conductance was applied; and (iii) we do measure the average response of all cells and possibly not all RBCs responded to the NS309 stimulation. Furthermore, inhibiting the Gárdos channel with TRAM34 results in a significant depolarization, proving the involvement of the Gárdos channel in the membrane potential jump. For TritonX-100, please refer to panel A. In Panel C we show, that a similar Gárdos channel-mediated hyperpolarization can be induced by increasing the intracellular Ca^{2+} concentration with an application of the Ca^{2+} ionophore A23187, i.e., Ca^{2+} enters the cell and acts as the natural agonist of the Gárdos channel. Again, depolarization upon the addition of TRAM34 proves the contribution of the Gárdos channel. Finally, in panel D, we activate Piezo1, which allows Ca^{2+} entry and thus the activation of the Gárdos channel demonstrating the interplay between Piezo1 and the Gárdos channel. Once more, the addition of TRAM34 induces depolarization.

Preprints (www.preprints.org) | NOT PEER-REVIEWED | Posted: 17 October 2023 doi:10.20944/preprints202310.1044.v1

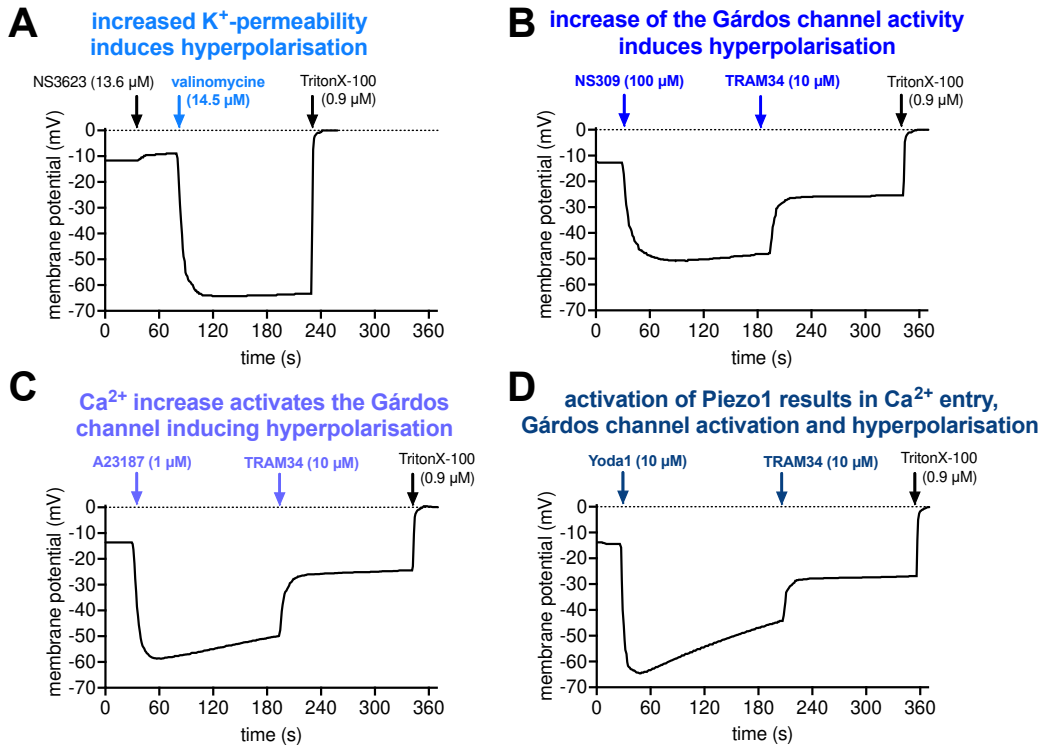

Figure 5. Effect of Gárdos channel and Piezo1 activation on the membrane potential. Panel A represents RBCs, where first the Cl^- conductance is blocked with NS3623 and then a K^+ conductance is induced by the addition of valinomycin. The hyperpolarisation can therefore be regarded as fully based on the K^+ conductance. The experimental solution contained 146 mM NaCl and 9.9 mM KCl. Panel B shows the hyperpolarisation of the cells upon the addition of the Gárdos channel activator NS309. Please note that NS309 only increases the Ca^{2+}-sensitivity of the Gárdos channel and hence its open probability, i.e. not all Gárdos channels are open and neither are all RBCs hyperpolarised. The experimental solution was an ordinary Ringer solution (154 mM NaCl and 2 mM KCl). Panel C shows the hyperpolarisation of the RBCs caused by an increase in intracellular Ca^{2+} concentration by the addition of the Ca^{2+} ionophore 4-bromo-A23187 (A23187) inducing the activation of the Gárdos channel. Panel D shows the hyperpolarisation of the cells after activation of Piezo1 by Yoda1, which results in Ca^{2+} entry and hence Gárdos channel activation. All experiments are performed in ordinary Ringer solution, i.e. are nominal Ca^{2+}-free, but due to impurities containing an estimated Ca^{2+} concentration of at least 4 µM [53]. All panels show representative curves of at least duplicate measurements of at least 3 healthy donors.

3. Discussion

3.1. The copy number of ion channels in red blood cells – context and consequences

For the most prominent ion channels in the RBC membrane, the Gárdos channel and Piezo1, we could show that they are still at or below the detection limit using state-of-the-art biochemical detection methods (transcriptomics, proteomics, and antibody-based flow cytometry). This is in line with patient investigations showing an explicit haematological phenotype when carrying pathological variants of the Gárdos channel or Piezo1 [14,30,33–36,40–42,48]. The same holds true for transgenic approaches in animal models [3,5,45,54,55]. Of note, there are other ion channels in RBC with strong functional evidence for their existence but controversial biochemical detection and electrophysiological measurements are impossible or difficult to realize such as for Cav2.1 [14,56–58] or TRPC6 [11,58–60].

In all of the examples above, it is the low copy number of the ion channel in the RBC membrane that is the major obstruction, a lot due to the fact that RBCs lack protein translation [61]. Thus there is the necessity to discriminate between the physical presence of a protein, which may still be

 doi:10.20944/preprints202310.1044.v1

recognized by an antibody while the function of the protein might be lost at some point in the in average 120 days lifetime of a RBC in the circulation [62] or *vice versa* when proteins might not be physically detected while functional evidence for their presence is at hand like in our study showing below-limit mass spectrometry LFQ values for the Gárdos channel.

Considering all these circumstances it is not surprising, that most of the patch-clamp-based reports on RBCs represent cherry-picking results hiding the success rate and/or yield of measured channels with very few exceptions, e.g. [21,63]. Especially for the Gárdos channel, the majority of published recordings are performed as 'inside-out patches' (single channel recordings) and only very few as 'whole-cell recordings', e.g. [33,64], based mostly on patients suffering from hereditary anaemias with an, in average, younger RBC population. In this respect the data presented here, we consider as a 'round up' of previous reports. Based on the patch-clamp measurements presented in this report, we estimated the channel numbers for the Gárdos channel based on the whole-cell conductance (122 pS for reticulocytes and 55 pS for mature RBCs; Figure 3B) and a single channel conductance of 18 pS [16,17] of being 6.8 and 3.1 in reticulocytes and mature RBCs, respectively, for cells classified as responders. Considering the proportion of non-responders (33.3% for reticulocytes and 40% for mature RBCs; Figure 3C), the average number of NS309-activatable number of Gárdos channels per cell drops to 4.5 and 1.8 in reticulocytes and mature RBCs, respectively. This is in rough agreement with previous reports [21,37] as outlined in the Introduction. For Piezo1 we have statistical data only for particular voltages such as 80 mV (Figure 4C). Based on a Piezo1 single channel conductance of 29 pS [65], the current of a single channel at 80 mV corresponds to 2.3 pA. This in turn results in a Yoda1-activatable number of fully activated channels of 35 and approximately 65 for reticulocytes and mature RBCs, respectively. (For a discussion of why mature RBCs show higher activity, see below.) Considering the proportion of non-responders (72.5% for reticulocytes and 81% for mature RBCs; Figure 4D), the average number of Yoda1 (in the presence of TRAM34) activatable number of Piezo1 channels per cell drops to 9.5 and 5.8 in reticulocytes and mature RBCs, respectively. Thus, the number of activatable Piezo1 channels is considerably higher than that of activatable Gárdos channels but still within the same order of magnitude. Please note, the number of activatable channels measured by patch-clamp my not represent thy physical number of channel copies.

On the other hand, the low copy number of activatable channels enables membrane potential jumps (polarization-depolarization cycles) [66]: Based on the low K^+ conductance of the RBC membrane, resulting in setting the RBC resting membrane potential on the distribution of the chloride ions, openings of the Gárdos channels result in hyperpolarization (cp. Figure 5) and if followed by closures in depolarizations. The low copy number of the Gárdos channels in combination with the stochastic channel openings (cp. Figure A1) allows those membrane potential jumps. In analogy to action potentials but considering the non-excitable nature of RBCs we call this phenomenon 'pseudo action potentials' (PAPs). In turn, PAPs enable the activation of voltage-gated channels [14,67].

3.2. Ion channel interactions in red blood cells and their physiological function

As mentioned above the activity of the Gárdos channel may drive voltage-activated channels, which in turn can be suppressed by Piezo1 activity [14,67], (compare opaque elements in Figure 6A). However, next we like to focus the discussion on the dualism between the Gárdos channel and Piezo1 (Figure 6).

Preprints (www.preprints.org) | NOT PEER-REVIEWED | Posted: 17 October 2023 doi:10.20944/preprints202310.1044.v1

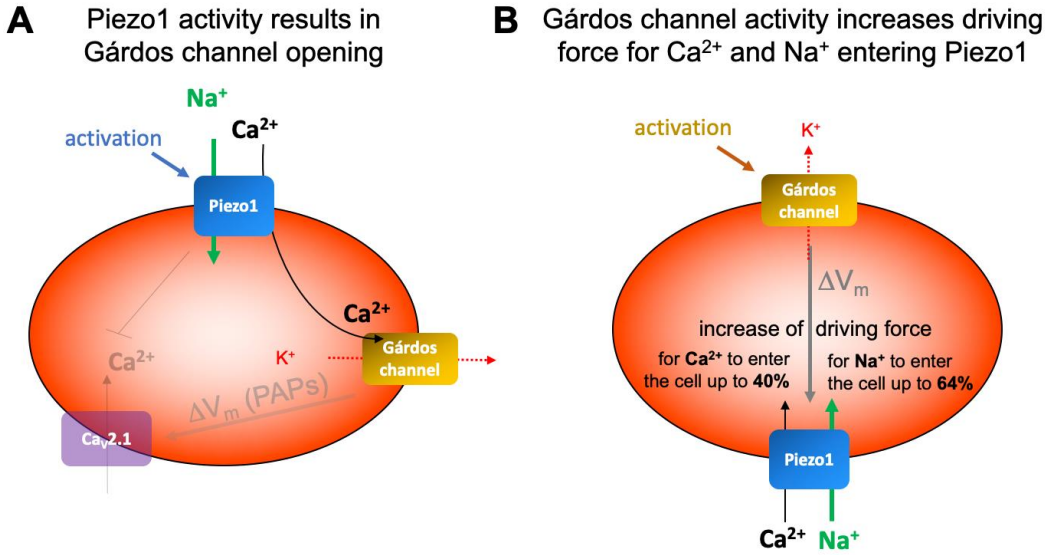

Figure 6. Schematic presentation of the interplay of Gárdos channel and Piezo1. Panel A shows the impact of Piezo1 on the Gárdos channel and in opaque the effect of the Gárdos channel (and to some extent the Piezo1) on the voltage-activated calcium channel Cav2.1 [14,56–58]. Panel B indicates the putative effect of Gárdos channel openings on Piezo1. For further details see main text.

The hypothesis that Piezo1 activity, which leads to a Ca^{2+} entry is followed by Gárdos channel activation (Figure 6A), is in the meantime an established concept, e.g. [3–5,12,45,68]. Can this be recognized also in patch-clamp measurements? In inside-out patches, where only a membrane patch covers the pipette tip, the volume in the bath is so much higher than in the cell and without diffusion barriers, the dilution of the Ca^{2+} entering through Piezo1 is immediate and hence no activation of the Gárdos channel is possible. Regarding whole-cell measurements, although the inner RBC volume is connected to – again – the very large volume of the patch pipette, activation of the Gárdos channel must be considered and therefore all our Piezo1 measurements were performed in the absence and presence of the Gárdos channel inhibitor TRAM34 (Figure 4). While for the reticulocytes we saw a small insignificant current decrease in the presence of TRAM34, which might be caused by hindering of immediate Ca^{2+} dilution by diffusion barriers (internal structures, e.g., mitochondria), such a decrease was absent in the organelle-free mature RBCs (Figure 4C). However, the lack of Gárdos channel activation following Piezo1 activation in patch-clamp measurements was shown before [48] and can well be attributed as a patch-clamp measurement limitation. In contrast, the MBE measurements in intact cells, clearly demonstrate the Gárdos channel opening after Piezo1 activation (Figure 5D). As a side note, Figures 5C and 5D nicely demonstrate that in the nominal absence of Ca^{2+}, the Ca^{2+} 'contamination' of solutions even when using analytical grade chemicals, we estimate a 4-8 µM, is sufficient to activate the Gárdos channel [53].

Vice versa we noticed an increase in current after TRAM34 application, which was also previously reported [48]. Although we don't have a comprehensive explanation for this effect, we like to point to another problem, which arises from the small copy number the ion channels in RBCs, that is the abundance of pharmacological side effects. Most drugs cause such side effects and if the number of channels is very small, the side effects could (in contrast to overexpressing systems, where drugs are usually tested) overwhelm the intended effect of a particular drug as, e.g., shown for TRPC6 inhibitors on RBCs [58].

In addition to the effect of Piezo1 on the Gárdos channel (Figures 5D and 6A), there is also an influence of the Gárdos channel on Piezo1, which originates from the hyperpolarization caused by the Gárdos channel (Figures 5B and 4C) and which is visualized in Figure 6B. The electrochemical gradient is the driving force for a particular ion to cross the membrane. It is the sum of the chemical potential, caused by the unequal distribution of the ion on both sides of the membrane, which can be

Preprints (www.preprints.org) | NOT PEER-REVIEWED | Posted: 17 October 2023 doi:10.20944/preprints202310.1044.v1

calculated by the Nernst equation (see equation 1, above) and the electrical driving force which is caused by the distribution of all ions and their membrane permeability. The electical driving force was measured in the experiments shown in Figure 5 and can be calculated by the Goldman-Hodgkin-Katz equation (equation 2, see below). The potentials acting on particular ions are summarized in Table 1 and given for the resting membrane potential (approximately -12 mV) and for the membrane potential after Gárdos channel activation (hyperpolarization, approximately -70 mV) – compare Figure 5.

Table 1. Driving forces for particular cations for the measured resting membrane potential (-12 mV) and after opening of the Gárdos channel (-70 mV).

ion	Ca^{2+}	Na^{+}	K^{+}
extracellular concentration	1.2 mM [69]	140 mM [70]	4 mM [71]
intracellular concentration	60 nM [72]	7.35 mM [73]	102 mM [52]
chemical potential*	-132 mV	-79 mV	86 mV
electrochemical potential at resting membrane potential	-144 mV	-91 mV	74 mV
electrochemical potential when Gárdos channel is open	-202 mV	-149 mV	16 mV

* The chemical potential was calculated using the Nernst equation (equation 1). A negative potential in the table means the cations enter the cell and a positive potential means the cations exit the cell.

However, are the potentials given in Table 1 applicable for ion transport through Piezo1? The situation is a bit more complex, because in the moment Piezo1 is open, the membrane potential is also influenced by the permeability changes caused by Piezo1. Therefore, the electrochemical potentials given in Table 1 denote the boundaries within the membrane potential may adjust. The actual membrane potential is defined by the Goldman-Hodgkin-Katz equation:

$$V_m = \frac{RT}{F} \times \ln \frac{\sum_i^n P_{M_i^+} \left[M_i^+\right]_{out} + \sum_j^m P_{A_j^-} \left[A_j^-\right]_{in}}{\sum_i^n P_{M_i^+} \left[M_i^+\right]_{in} + \sum_j^m P_{A_j^-} \left[A_j^-\right]_{out}} \quad (2)$$

where M^+ are monovalent cations, A^- are monovalent anions with P being the permeability of the indexed ion. For illustrative purpose equation 2 with just considering Na^+, K^+ and Cl^- ions would read:

$$V_m = \frac{RT}{F} \times \ln \frac{P_{Na}[Na^+]_{out} + P_K[K^+]_{out} + P_{Cl}[Cl^-]_{in}}{P_{Na}[Na^+]_{in} + P_K[K^+]_{in} + P_{Cl}[Cl^-]_{out}} \quad (3)$$

In these equations the permeability P is crucial, i.e. the distinct number of available functional Piezo1 and Gárdos channels determine the cell permeability and hence the membrane potential.

To better judge the situation, we like to include one more aspect into the discussion, which is the opening time (interval) of the channels. As mentioned before, Piezo1 has a transient opening behavior. In intact RBCs this transient opening is obviously sufficient to have enough Ca^{2+} to enter the cell for an activation of the Gárdos channel. The dominating K^+-loss leads to volume adaptations in particular cell shrinkage, e.g., to allow RBCs to pass small capillaries or the sinusoidal slits in the spleen following mechanical stress [3–5,74]. Although Piezo1 and TRPV2 share a number of properties [75] such as being nonselective cation channels and having the same magnitude of the single channel conductance, the activation of the two channels has different consequences. Activation of TRPV2, e.g., by Δ^9-tetrahydrocannabinol [76], results in longer opening times and although Ca^{2+} is expected to enter the RBC and activate the Gárdos channel, due to different driving forces (compare Table 1), the Na^+ entry trough TRPV2 dominates the K^+ exit through the Gárdos channel with the result that RBCs swell [77,78]. This shows that (patho)physiological effects can be tuned in opposite directions by a single biophysical property of a channel, such as the transient nature of the opening.

3.3. Ion channel differences between reticulocytes and mature red blood cells

 doi:10.20944/preprints202310.1044.v1

We do see differences in ion channel function between reticulocytes and mature RBCs for both channels, the Gárdos channel and Piezo1, but opposite trends.

For the Gárdos channel even when considering that reticulocytes have a 20% bigger surface area than mature RBCs in average [73] still the current density is double the size in reticulocytes compared to mature RBCs. In accordance the number of responding cells drops from 67% to 60%. This decrease in activity is somehow expected because of the lack of protein translation and the protein 'aging' [61]. It is also in line with data in the literature, showing age-dependent changes in RBC composition, metabolism and transport [79–81].

Surprisingly, the trend of the current density differences between reticulocytes and mature RBCs for Piezo1 is opposite to the Gárdos channel, i.e. increasing in mature RBCs albeit the mature RBCs contain 20% less membrane [73]. Although this difference is not significant and one should be careful with an 'over interpretation', a plausible explanation arises from the fact that Piezo1 activity is modulated by the lipid composition of the membrane the channel is embedded in [82–84] and there is a severe lipid remodelling associated with the ageing process all the way from reticulocytes to senescent RBCs [85]. This remodelling process may at least partly explain the cellular heterogeneity indicated by the fairly large error bars in Figure 4C. The protein ageing process used as an argument when describing the Gárdos channel would also apply to Piezo1 and is indeed reflected in the number of responding cells, which drops from 35±5% (reticulocytes) to 8±2% (mature RBCs) p=0.002.

4. Materials and Methods

4.1. Blood collection

Blood collection was performed following the declaration of Helsinki and was approved by the ethics committee of 'Ärztekammer des Saarlandes', permit number 51/18. Blood was collected from healthy donors into heparin tubes by venipuncture, washed, and resuspended. Washing of full blood samples was carried out at 1800×g for 6 min prior to the procedures described below.

4.2. Transcriptome analysis

To purify human RBCs we followed a method originally developed by Beutler et al. [86]. Blood samples were centrifuged at 1000xg for 20 min. Plasma was aspirated and mixed with phosphate buffered saline (PBS) (1:10). RBCs were washed 3 times (1000xg, 5 min) and mixed with PBS (1:1). Filter paper (Whatman No. 4 GE Healthcare, UK) was pressed in a 10 ml syringe (Omnifix Solo Lure, Germany) and a mixture of 180 mg Sigma- and 180 mg Alpha-Cellulose (Sigma-Aldrich, USA) suspended in 10 ml PBS was added. After the PBS drained, the syringe was primed with 10 ml of the diluted plasma. One ml of RBCs was added and eluted with 10 ml PBS. Filtered RBCs were again washed 3 times in PBS. For a following RNA isolation RBCs were used immediately.

To evaluate the purification of the RBCs we used the gelatin zymography technique [87]. This method allows the detection of contaminations with polymorphonuclear neutrophils (PMNs), a type of leucocytes that cannot be eliminated by washing the blood sample. PMNs are the only type of blood cells that express the matrix metalloproteinase 9 (MMP-9), whose catalytic activity against gelatin can be used as a specific marker.

Briefly, 10 µl of diluted RBCs samples (PBS, 1:10) were lysed by adding Zymogram Tris-Glycine SDS Sample Buffer (1:1) (Thermo Fisher Scientific, USA), followed by a protein separation in 10% Gelatin Protein Gels (Thermo Fisher Scientific, USA) using a nonreducing SDS-PAGE. After separation (2 h, 125 V), gels were incubated for 1 h in Zymogram Renaturing Buffer (Thermo Fisher Scientific, USA) under continuous shaking and washed three times in Aqua dest. For activation of the catalytic activity of MMP-9, the gels were incubated for up to 40 h in a digestion buffer containing (in mM): 50 Tris-HCl pH 7.6, 150 NaCl, 10 $CaCl_2$. Degradation of gelatin in the gel could be visualized after Coomassie blue staining as white spots.

For leucocyte depletion we used antibody-coupled magnetic beads. To reduce the number of $CD45^+$ cells that needed to be eliminated we first performed the Ficoll-Paque separation of the blood sample. Blood was diluted with PBS and layered on top of the Ficoll-Paque solution (GE Healthcare,

 doi:10.20944/preprints202310.1044.v1

UK). After centrifugation (800xg, 25 min) plasma and a layer of leucocytes were removed and RBCs were washed three times in isolation buffer (PBS with 0.1% BSA and 2 mM EGTA). Cells were incubated over night at 4°C with the following antibodies: IgG rabbit anti human CD45 (GeneTex Inc., USA) [1:40] and IgG rabbit anti human CD15 (Biorbyt, UK) [1:50]. Magnetic beads (Dynabeads sheep anti-rabbit, Thermo Fisher Scientific, USA) were washed once in isolation buffer using a DynaMag Holder (Thermo Fisher Scientific, USA) and then added to the RBCs (1:1) for further 120 min. To remove the bead-bound cells the RBC-Bead-Mix was washed twice in PBS again using the DynaMag Holder. For RNA isolation we used the RiboPure RNA Purification Kit (Thermo Fisher Scientific, USA) and 500 µl of human blood samples, prepared as described before. Subsequently, the alpha and beta globin mRNA, which have the highest expression in reticulocytes, was removed from the total RNA preparations by using the GLOBINclear Kit (Thermo Fisher Scientific, USA) according to the manufacturer´s protocol. Transcriptome analysis was performed by Expression Analysis Inc. (USA) using next-generation sequencing.

4.3. Proteomic analysis

Samples were lysed in 8 M urea (Life technologies, USA) in 100 mM TRIS-HCl pH 8 (Life technologies, USA). Sample prep was started with input of 10 µg protein. Disulfide bonds were reduced with 10 mM DTT (Life technologies, USA) for 60 minutes at 20°C, alkylated with 55 mM iodocetamide (Life technologies, USA) for 45 minutes at 20°C and samples were digested for 16 hours at 20°C with MS-grade trypsin (Promega, Germany) in a ratio of 1:20 trypsin : protein. Tryptic peptides were desalted and concentrated using Empore-C18 StageTips and eluted with 0.5% (v/v) acetic acid, 80% (v/v) acetonitrile. Sample volume was reduced by SpeedVac and supplemented with 2% acetonitrile, 0.1% TFA to a final volume of 5 µl. 3 µl of each sample was injected for mass spectrometry analysis.

Tryptic peptides were separated by nanoscale C18 reverse phase chromatography coupled on line to an Orbitrap Fusion Tribrid mass spectrometer (Thermo Scientific, USA) via a nanoelectrospray ion source (Nanospray Flex Ion Source, Thermo Scientific, USA). Peptides were loaded on a 20 cm, 75–360 µm inner-outer diameter fused silica emitter (New Objective) packed in-house with ReproSil-Pur C18-AQ, 1.9 µm resin (Dr. Maisch GmbH, Germany). The column was installed on a Dionex Ultimate3000 RSLC nanoSystem (Thermo Scientific, USA) using a MicroTee union formatted for 360 µm outer diameter columns (IDEX) and a liquid junction. The spray voltage was set to 2.15 kV. Buffer A was composed of 0.5 % acetic acid and buffer B of 0.5 % acetic acid, 80% acetonitrile. Peptides were loaded for 17 minutes at 300 nl/min at 5% buffer B, equilibrated for 5 minutes at 5% buffer B (17-22 min) and eluted by increasing buffer B from 5-15% (22-87 min) and 15-38% (87-147 min), followed by a 10-minute wash to 90% and a 5-minute regeneration to 5%. Survey scans of peptide precursors from 400 to 1500 m/z were performed at 120K resolution (at 200 m/z) with a 1.5×10^5 ion count target. Tandem mass spectrometry was performed by isolation with the quadrupole with an isolation window 1.6, HCD fragmentation with a normalized collision energy of 30, and rapid scan mass spectrometry analysis in the ion trap. The MS^2 ion count target was set to 1.5×10^4 and the max injection time was 35 ms. Only those precursors with charge states 2–7 were sampled for MS^2. The dynamic exclusion duration was set to 60 seconds with a 10 ppm tolerance around the selected precursor and its isotopes. Monoisotopic precursor selection was turned on. The instrument was run in top speed mode with 3 s cycles. All data were acquired with Xcalibur software.

Mass spectrometry raw files were processed with MaxQuant 2.0.1.0 [88] using the human Uniprot database (downloaded March 2021). MaxQuant output tables were analyzed using R/Bioconductor (version 4.1.2/3.14) [89], 'reverse', 'potential contaminants' and 'only identified by site' peptides were filtered out and label free quantification values were $\log_2$ transformed. Raw MS files and search/identification files obtained with MaxQuant have been deposited in the ProteomeXchange Consortium [90] via the PRIDE partner repository with the dataset identifier PXDxxxxx.

4.4. PBMC isolation and culture

Preprints (www.preprints.org) | NOT PEER-REVIEWED | Posted: 17 October 2023 doi:10.20944/preprints202310.1044.v1

Peripheral blood (~25 ml) was collected in Li-heparin tubes (Sarstedt, Germany). PBMC were isolated using Ficoll Histopaque (density=1.077 g/ml, 20°C; GE Healthcare, USA) following the manufacturer's protocol. Remaining RBCs in the cell isolate were lysed (lysis buffer=155 mM NH_4Cl, 12 mM $KHCO_3$, 0.1 mM EDTA; 10 min at room temperature). PBMC were cultured as previously described [91]. In short, a two-phase culture system was employed for *in vitro* erythropoiesis: in the expansion phase, PBMC (day 0 expansion) were cultured in CellQuin medium supplemented with EPO (2 IU/ml; Prospec, USA), dexamethasone (1 µM; Sigma-Aldrich, USA) and human stem cell factor (hSCF; 100 ng/ml, ITK diagnostics, The Netherlands). The differentiation phase was started at day 13 expansion by washing the cells once with PBS and reseeding them in CellQuin supplemented with human plasma (5% v/v; Octapharma GmbH, Germany), EPO (10 IU/ml), heparin (5 IU/ml; MP Biomedicals™, USA) and additional holotransferrin (final concentration of 1000 µg/ml; Sanquin, The Netherlands). All cultures were kept in humidified incubators (at 37°C, air plus 5% carbon dioxide). Cell concentration was regularly determined using a CASY cell counter (CASY Model TCC, OLS OMNI Life Science, Germany). In case cell were shipped, they were suspended in MOD6 buffer (Sanquin, The Netherlands).

4.5. Flow Cytometry

Cultured cells or isolated RBCs were washed with PBS (5 min, 600xg), stained with primary antibody or reagents (20 min, room temperature), washed and resuspended in flow cytometry buffer (5 min, 600xg), and measured in a FACS Canto™II flow cytometer (BD Biosciences, USA). Antibodies used were CD71-PB (1:100 dilution; Miltenyi Biotec, Germany) and KCa3.1 (SK4) (1:100 dilution; Abgent, USA). Gating was done against specific isotype controls: anti-mouse isotype control IgG1k-pacific blue (1:200; Biolegend, USA) and anti-mouse isotype control IgG1- PE, (1:200; R&D Systems, USA). The obtained data were analyzed with Flowjo™ (BD Biosciences, USA).

4.6. Patch-clamp measurements

Patch-clamp measurements were performed with automated systems based on planar chips, the Patchliner for the Gárdos channel assay and the SyncroPatch 384 for the Piezo1 measurements (both: Nanion Technologies, Munich, Germany). Recordings were performed at room temperature using planar borosilicate glass patch clamp chips for the respective devises with resistances of 5-8 MΩ (Patchliner) and 9-12 MΩ (SyncroPatch 384). The internal and external solutions used to measure the Gárdos channel were (in mM): KCl 70, KF 70, HEPES 30, EGTA 3, $CaCl_2$ 0.61, pH=7.2 adjusted with KOH (internal) and KCl 140, $MgCl_2$ 5, $CaCl_2$ 6, D-glucose 2.5, HEPES 10, pH=7.3 adjusted with KOH (external). The internal and external solutions used to measure Piezo1 were (in mM): KCl 10, KF 110, NaCl 10, EGTA 10 and HEPES 10, pH=7.2 adjusted with KOH (internal) and NaCl 140, KCl 4, $CaCl_2$ 2, $MgCl_2$ 1, Glucose 5 and HEPES 10, pH=7.3 adjusted with KOH (external).

Gigaseal formation was facilitated by the use of a seal-enhancing solution as recommended by the Patchliner manufacturer and containing (in mM): NaCl 80, KCl 3, $MgCl_2$ 10, $CaCl_2$ 35, HEPES 10, pH=7.3 adjusted with NaOH. The seal-enhancing solution was only used to help obtain the very high gigaohmic contact between the cell and the chip and in the whole-cell configuration was replaced by the external solution. Whole-cell configuration was achieved by negative pressure suction pulses between -45 mbar and -150 mbar and its formation was judged by the appearance of sharp capacitive transients. Whole-cell patch-clamp recordings of the Gárdos channel were conducted using voltage steps from -110 mV to 30 mV for 500 ms in 20 mV increments at 5 s intervals, the holding potential being set at -30 mV. Gárdos current differences between erythrocytes and reticulocytes were evaluated with the use of NS-309 (100 µM), a specific activator of the channel. Whole cell currents of Piezo1 were elicited using a voltage ramp protocol (−100 mV to 80 mV, 450 ms, every 5 s, holding potential −30 mV). After recording a stable baseline current in external solution, cells were exposed to 10 µM Yoda1 (Tocris) for ~4 min, to investigate the activity of Piezo1 channels, followed by application of 30 µM GdCl3 (Sigma), a non-selective inhibitor of Piezo1. Where indicated, the selective Gárdos channel inhibitor TRAM-34 (2.5 µM, Tocris) was employed in combination with Yoda1. Only cells with seal resistance >0.5 GΩ were used for analysis. The compound-induced

Preprints (www.preprints.org) | NOT PEER-REVIEWED | Posted: 17 October 2023 doi:10.20944/preprints202310.1044.v1

current was obtained by subtracting the average of the last 3 sweeps obtained from the compound addition period and the average of the last 10 sweeps obtained from the reference addition period at 80 mV. If the mean current amplitude elicited upon compound addition exceeded 3σ of the mean current amplitude at baseline conditions, a cell was considered as responder.

4.7. The Macey-Bennekou-Egée (MBE) method

The membrane potential measurements of an RBC population were performed according to a method initially described by Macey *et al.* [92] further developed and applied by Poul Bennekou, e.g., Braunbæk and Bennekou 2008 [53] and kept alive by the laboratory of Stéphane Egée [34]. Therefore, we refer to it as the MBE-method.

For each experiment 1 ml of the Ringer solution (154 mM NaCl, 2 mM KCl) was poured into a 2 ml Eppendorf tube and a magnetic stir bar (VWR, cylindrical, 8x3mm) was added. Then, the protonophore carbonyl cyanide m-chlorophenyl hydrazone (CCCP, Sigma Aldrich, St. Luis, MO, USA) was added to reach a final concentration of 27 µM. The Eppendorf tube was placed in a 36°C water bath and a rotating magnet (990 rpm) was used to stir the sample. Now the calibrated pH meter (SevenCompact S210, Mettler-Toledo, Giessen, Germany) was immersed in the liquid (In Lab Solids pro- ISM, Mettler-Toledo, Giessen, Germany) to allow continuous measurements. The pH meter was connected to a personal computer and the values were measured every second and recorded by custom-designed software. One minute after the start of the recording, 150 µl of washed RBCs were pipetted into the Ringer's solution containing CCCP and after two minutes drugs according to the particular protocol were added. At the end of each experiment, TritonX-100 (Sigma Aldrich, St. Louis, MO, USA) was added to reach a final concentration of 0.9 µM to lyse the RBCs in order to calibrate the system for a membrane potential of 0 mV.

The stored data were transferred to Excel (Microsoft, Redmond, WA, USA) and the recorded pH values were transferred into a membrane potential using the formula:

$$V(mV) = -61.5 \times (pH_{out} - pH_{in}) \quad (4)$$

where, pH_{out} is the measured pH-value during the experiment and pH_{in} is the last measured calibration pH-value at the end of the recording after cell lysis.

Finally, the membrane potentials were plotted against time in the Prism 9 software (Graph Pad, San Diego, CA, USA).

5. Summary and Conclusions

Although both channels, the Gárdos channel and Piezo1 are at the detection limit of biochemical methods (Figure 1), they can be functionally studied by both, the patch-clamp technique (Figures 2-4) and the MBE method (Figure 5). With the patch-clamp technique differences between reticulocytes and mature RBCs could be detected for both channels (Figures 3&4). Activation of Piezo1 results in Ca^{2+}-mediated opening of the Gárdos channel but also *vice versa*, Gárdos channel activity provides changes in the driving force for ions passing Piezo1 (Figure 6).

Channel properties are extensively discussed to better understand their physiological function, which is volume adaptation when passing small constrictions such as small capillaries or sinusoidal slits of the spleen [4,93,94] as well as the signalling that leads to the active participation of RBCs in clot and thrombus formation [6,7,95,96].

Author Contributions: Conceptualization, L.K., S.E., M.v.L. and E.v.d.A.; methodology, P.P.K., N.M., J.J., T.J., G.S., G.I., M.Q., L.H., M.G.R., N.B. and S.E.; software, T.J.; formal analysis, P.P.K., N.M., J.J., G.S., G.I., M.Q., L.H., A.J.H. and M.G.R; investigation, P.P.K., N.M., J.J., G.S., G.I., M.Q., A.J.H. and L.H.; resources, C.W., M.v.L. and E.v.d.A.; data curation, L.K.; writing—original draft preparation, L.K.; writing—review and editing, all authors; visualization, P.P.K., N.M., J.J., G.S. and L.K.; supervision, M.G.R., N.B., C.W., M.v.L., E.v.d.A. and L.K.; project administration, E.v.d.A. and L.K.; funding acquisition, M.G.R., N.B., C.W., M.v.L., S.E., E.v.d.A. and L.K. All authors have read and agreed to the published version of the manuscript.

Funding: This work received funding by the Marie Skłodowska-Curie grant agreement no. 860436—EVIDENCE.

 doi:10.20944/preprints202310.1044.v1

Institutional Review Board Statement: The study involving human blood was conducted according to the guidelines of the Declaration of Helsinki and approved by the Ethics Committee of the "Ärztekammer des Saarlandes" (approval number 51/18).

Informed Consent Statement: Written informed consent was obtained from all subjects involved in the study.

Data Availability Statement: All relevant data are included in the article; further inquiries can be di-rected to the corresponding author. Source data files for the figures are provided in the supplementary material file.

Conflicts of Interest: The authors declare no conflict of interest.

Appendix A

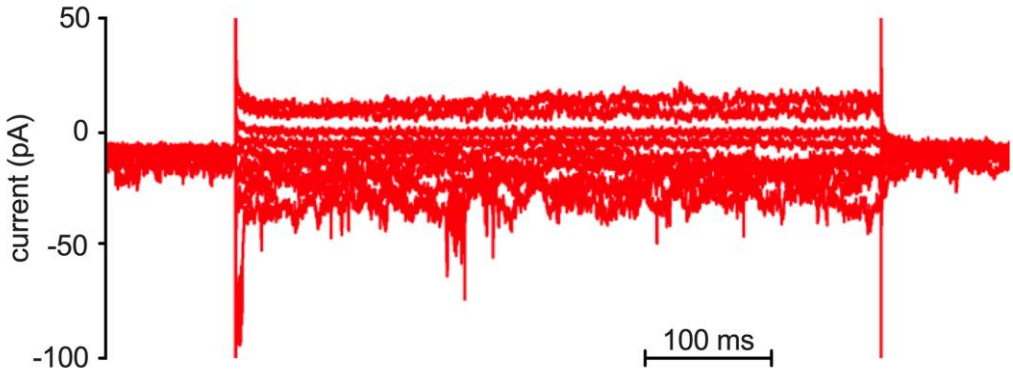

Figure A1. Example of patch-clamp recording of a red blood cell. Overlay of currents at various potentials (cp. Figure 2A) while stimulated with the Gárdos channel activator NS309. Although this is a whole-cell recording, single channel openings are visible in the flickering appearance of the current traces.

References

1. Thomas, S.L.Y.; Bouyer, G.; Cueff, A.; Egée, S.; Glogowska, E.; Ollivaux, C. Ion Channels in Human Red Blood Cell Membrane: Actors or Relics? *Blood Cells, Molecules, and Diseases* **2011**, *46*, 261–265, doi:10.1016/j.bcmd.2011.02.007.
2. Kaestner, L.; Bernhardt, I. Ion Channels in the Human Red Blood Cell Membrane: Their Further Investigation and Physiological Relevance. *Bioelectrochemistry* **2002**, *55*, 71–74.
3. Faucherre, A.; Kissa, K.; Nargeot, J.; Mangoni, M.; Jopling, C. Piezo1 Plays a Role in Erythrocyte Volume Homeostasis. *Haematologica* **2013**, *99*, doi:10.3324/haematol.2013.086090.
4. Danielczok, J.G.; Terriac, E.; Hertz, L.; Petkova-Kirova, P.; Lautenschläger, F.; Laschke, M.W.; Kaestner, L. Red Blood Cell Passage of Small Capillaries Is Associated with Transient Ca2+-Mediated Adaptations. *Front Physiol* **2017**, *8*, 979, doi:10.3389/fphys.2017.00979.
5. Cahalan, S.M.; Lukacs, V.; Ranade, S.S.; Chien, S.; Bandell, M.; Patapoutian, A. Piezo1 Links Mechanical Forces to Red Blood Cell Volume. *Elife* **2015**, *4*, doi:10.7554/elife.07370.
6. Andrews, D.A.; Low, P.S. Role of Red Blood Cells in Thrombosis. *Curr Opin Hematol* **1999**, *6*, 76–82.
7. Bernhardt, I.; Wesseling, M.C.; Nguyen, D.B.; Kaestner, L. Red Blood Cells Actively Contribute to Blood Coagulation and Thrombus Formation. In *Erythrocyte*; Tombak, A., Ed.; IntechOpen: London, 2019 ISBN 9781789842098.
8. Kaestner, L. Channelizing the Red Blood Cell: Molecular Biology Competes with Patch-Clamp. *Frontiers in molecular biosciences* **2015**, *2*, 46, doi:10.3389/fmolb.2015.00046.
9. Kaestner, L. Cation Channels in Erythrocytes - Historical and Future Perspective. *Open Biology J* **2011**, *4*, 27–34, doi:10.2174/1874196701104010027.
10. Petkova-Kirova, P.; Hertz, L.; Makhro, A.; Danielczok, J.; Huisjes, R.; Llaudet-Planas, E.; Mañú-Pereira, M. del M.; Corrons, J.-L.V.; Wijk, R. van; Bogdanova, A.; et al. A Previously Unrecognized Ca2+-Inhibited Nonselective Cation Channel in Red Blood Cells. *Hemasphere* **2018**, *2*, e146, doi:10.1097/hs9.0000000000000146.
11. Hertz, L.; Flormann, D.; Birnbaumer, L.; Wagner, C.; Laschke, M.W.; Kaestner, L. Evidence of in Vivo Exogen Protein Uptake by Red Blood Cells: A Putative Therapeutic Concept. *Blood Adv* **2023**, *7*, 1033–1039, doi:10.1182/bloodadvances.2022008404.
12. Hertz, L.; Huisjes, R.; Llaudet-Planas, E.; Petkova-Kirova, P.; Makhro, A.; Danielczok, J.G.; Egée, S.; Mañú-Pereira, M.D.M.; Wijk, R. van; Vives-Corrons, J.-L.; et al. Is Increased Intracellular Calcium in Red Blood

Cells a Common Component in the Molecular Mechanism Causing Anemia? *Frontiers in Physiology* **2017**, *8*, 673, doi:10.3389/fphys.2017.00673.
13. Badens, C.; Guizouarn, H. Advances in Understanding the Pathogenesis of the Red Cell Volume Disorders. *Br. J. Haematol.* **2016**, *174*, 674–685, doi:10.1111/bjh.14197.
14. Jansen, J.; Qiao, M.; Hertz, L.; Wang, X.; Fermo, E.; Zaninoni, A.; Colombatti, R.; Bernhardt, I.; Bianchi, P.; Kaestner, L. Mechanistic Ion Channel Interactions in Red Cells of Patients with Gárdos Channelopathy. *Blood Adv* **2021**, *5*, 3303–3308, doi:10.1182/bloodadvances.2020003823.
15. Yamaguchi, Y.; Allegrini, B.; Rapetti-Mauss, R.; Picard, V.; Garçon, L.; Kohl, P.; Soriani, O.; Peyronnet, R.; Guizouarn, H. Hereditary Xerocytosis: Differential Behavior of PIEZO1 Mutations in the N-Terminal Extracellular Domain Between Red Blood Cells and HEK Cells. *Front Physiol* **2021**, *12*, 736585, doi:10.3389/fphys.2021.736585.
16. Hamill, O.P. Potassium Channel Currents in Human Red Blood Cells. *J Physiol* **1981**, *319*, 97P-98P.
17. Hamill, O.P. Potassium and Chloride Channels in Red Blood Cells. In; Sakmann, B., Neher, E., Eds.; Single Channel Recording; 1983; pp. 451–471.
18. Gardos, G. The Permeability of Human Erythrocytes to Potassium. *Acta Physiol Hung* **1956**, *10*, 185–189.
19. Gardos, G. The Function of Calcium in the Potassium Permeability of Human Erythrocytes. *Biochim Biophys Acta* **1958**.
20. Dunn, P.M. The Action of Blocking Agents Applied to the Inner Face of Ca(2+)-Activated K+ Channels from Human Erythrocytes. *J Membr Biol* **1998**, *165*, 133–143.
21. Grygorczyk, R.; Schwarz, W.; Passow, H. Ca2+-Activated K+ Channels in Human Red Cells. Comparison of Single-Channel Currents with Ion Fluxes. *Biophys J* **1984**, *45*, 693–698, doi:10.1016/s0006-3495(84)84211-3.
22. Grygorczyk, R.; Schwarz, W. Ca2+-Activated K+ Permeability in Human Erythrocytes: Modulation of Single-Channel Events. *Eur Biophys J* **1985**, *12*, 57–65.
23. Grygorczyk, R.; Schwarz, W. Properties of the CA2+-Activated K+ Conductance of Human Red Cells as Revealed by the Patch-Clamp Technique. *Cell Calcium* **1983**, *4*, 499–510.
24. Schwarz, W.; Grygorczyk, R.; Hof, D. Recording Single-Channel Currents from Human Red Cells. *Methods Enzymol* **1989**, *173*, 112–121.
25. Grygorczyk, R. Temperature Dependence of Ca2+-Activated K+ Currents in the Membrane of Human Erythrocytes. *Biochim Biophys Acta* **1987**, *902*, 159–168.
26. Leinders, T.; Kleef, R.G. van; Vijverberg, H.P. Distinct Metal Ion Binding Sites on Ca(2+)-Activated K+ Channels in inside-out Patches of Human Erythrocytes. *Biochim Biophys Acta* **1992**, *1112*, 75–82.
27. Leinders, T.; Kleef, R.G.D.M.; Vijverberg, H.P.M. Single Ca2+-Activated K+ Channels in Human Erythrocytes: Ca2+ Dependence of Opening Frequency but Not of Open Lifetimes. *Biochimica Et Biophysica Acta Bba - Biomembr* **1992**, *1112*, 67–74, doi:10.1016/0005-2736(92)90255-k.
28. Hoffman, J.F.; Joiner, W.; Nehrke, K.; Potapova, O.; Foye, K.; Wickrema, A. The HSK4 (KCNN4) Isoform Is the Ca2+-Activated K+ Channel (Gardos Channel) in Human Red Blood Cells. *Proc Natl Acad Sci U S A* **2003**, *100*, 7366–7371, doi:10.1073/pnas.1232342100.
29. Lindern, M. von; Egée, S.; Bianchi, P.; Kaestner, L. The Function of Ion Channels and Membrane Potential in Red Blood Cells: Toward a Systematic Analysis of the Erythroid Channelome. *Front Physiol* **2022**, *13*, 824478, doi:10.3389/fphys.2022.824478.
30. Rapetti-Mauss, R.; Lacoste, C.; Picard, V.; Guitton, C.; Lombard, E.; Loosveld, M.; Nivaggioni, V.; Dasilva, N.; Salgado, D.; Desvignes, J.-P.; et al. A Mutation in the Gardos Channel Is Associated with Hereditary Xerocytosis. *Blood* **2015**, *126*, 1273–1280, doi:10.1182/blood-2015-04-642496.
31. Rapetti-Mauss, R.; Picard, V.; Guitton, C.; Ghazal, K.; Proulle, V.; Badens, C.; Soriani, O.; Garçon, L.; Guizouarn, H. Red Blood Cell Gardos Channel (KCNN4): The Essential Determinant of Erythrocyte Dehydration in Hereditary Xerocytosis. *Haematologica* **2017**, *102*, e415–e418, doi:10.3324/haematol.2017.171389.
32. Rapetti-Mauss, R.; Soriani, O.; Vinti, H.; Badens, C.; Guizouarn, H. Senicapoc: A Potent Candidate for the Treatment of a Subset of Hereditary Xerocytosis Caused by Mutations in the Gardos Channel. *Haematologica* **2016**, *101*, haematol.2016.149104, doi:10.3324/haematol.2016.149104.
33. Fermo, E.; Bogdanova, A.; Petkova-Kirova, P.; Zaninoni, A.; Marcello, A.P.; Makhro, A.; Hanggi, P.; Hertz, L.; Danielczok, J.; Vercellati, C.; et al. "Gardos Channelopathy": A Variant of Hereditary Stomatocytosis with Complex Molecular Regulation. *Scientific reports* **2017**, *7*, 1744, doi:10.1038/s41598-017-01591-w.
34. Fermo, E.; Monedero-Alonso, D.; Petkova-Kirova, P.; Makhro, A.; Pérès, L.; Bouyer, G.; Marcello, A.P.; Longo, F.; Graziadei, G.; Barcellini, W.; et al. Gardos Channelopathy: Functional Analysis of a Novel KCNN4 Variant. *Blood Adv* **2020**, *4*, 6336–6341, doi:10.1182/bloodadvances.2020003285.
35. Glogowska, E.; Lezon-Geyda, K.; Maksimova, Y.; Schulz, V.P.; Gallagher, P.G. Mutations in the Gardos Channel (KCNN4) Are Associated with Hereditary Xerocytosis. *Blood* **2015**, *126*, 1281–1284, doi:10.1182/blood-2015-07-657957.

36. Andolfo, I.; Russo, R.; Manna, F.; Shmukler, B.E.; Gambale, A.; Vitiello, G.; Rosa, G.D.; Brugnara, C.; Alper, S.L.; Snyder, L.M.; et al. Novel Gardos Channel Mutations Linked to Dehydrated Hereditary Stomatocytosis (Xerocytosis). *Am J Hematol* **2015**, *90*, 921–926, doi:10.1002/ajh.24117.
37. Wolff, D.; Cecchi, X.; Spalvins, A.; Canessa, M. Charybdotoxin Blocks with High Affinity the Ca-Activated K+ Channel of Hb A and Hb S Red Cells: Individual Differences in the Number of Channels. *J Membr Biology* **1988**, *106*, 243–252, doi:10.1007/bf01872162.
38. Coste, B.; Mathur, J.; Schmidt, M.; Earley, T.J.; Ranade, S.; Petrus, M.J.; Dubin, A.E.; Patapoutian, A. Piezo1 and Piezo2 Are Essential Components of Distinct Mechanically Activated Cation Channels. *Science* **2010**, *330*, 55–60, doi:10.1126/science.1193270.
39. Coste, B.; Xiao, B.; Santos, J.S.; Syeda, R.; Grandl, J.; Spencer, K.S.; Kim, S.E.; Schmidt, M.; Mathur, J.; Dubin, A.E.; et al. Piezo Proteins Are Pore-Forming Subunits of Mechanically Activated Channels. *Nature* **2012**, *483*, 176–181, doi:10.1038/nature10812.
40. Albuisson, J.; Murthy, S.E.; Bandell, M.; Coste, B.; Louis-dit-Picard, H. eacute l egrave ne; Mathur, J.; ant-Thibault, M.F. eacute n eacute; Tertian, G. eacute rard; Jaureguiberry, J.-P. de; Syfuss, P.-Y.; et al. Dehydrated Hereditary Stomatocytosis Linked to Gain-of-Function Mutations in Mechanically Activated PIEZO1 Ion Channels. *Nature communications* **2013**, *4*, 1–8, doi:10.1038/ncomms2899.
41. Zarychanski, R.; Schulz, V.P.; Houston, B.L.; Maksimova, Y.; Houston, D.S.; Smith, B.; Rinehart, J.; Gallagher, P.G. Mutations in the Mechanotransduction Protein PIEZO1 Are Associated with Hereditary Xerocytosis. *Blood* **2012**, *120*, 1908–1915, doi:10.1182/blood-2012-04-422253.
42. Bae, C.; Gnanasambandam, R.; Nicolai, C.; Sachs, F.; Gottlieb, P.A. Xerocytosis Is Caused by Mutations That Alter the Kinetics of the Mechanosensitive Channel PIEZO1. *Proceedings of the National Academy of Science of the United States of America* **2013**, *110*, E1162-8, doi:10.1073/pnas.1219777110.
43. Syeda, R.; Xu, J.; Dubin, A.E.; Coste, B.; Mathur, J.; Huynh, T.; Matzen, J.; Lao, J.; Tully, D.C.; Engels, I.H.; et al. Chemical Activation of the Mechanotransduction Channel Piezo1. *Elife* **2015**, *4*, e07369, doi:10.7554/elife.07369.
44. Picard, V.; Guitton, C.; Thuret, I.; Rose, C.; Bendelac, L.; Ghazal, K.; Aguilar-Martinez, P.; Badens, C.; Barro, C.; Bénéteau, C.; et al. Clinical and Biological Features in PIEZO1 -Hereditary Xerocytosis and Gardos Channelopathy: A Retrospective Series of 126 Patients. *Haematologica* **2019**, *104*, 1554–1564, doi:10.3324/haematol.2018.205328.
45. Ma, S.; Cahalan, S.; LaMonte, G.; Grubaugh, N.D.; Zeng, W.; Murthy, S.E.; Paytas, E.; Gamini, R.; Lukacs, V.; Whitwam, T.; et al. Common PIEZO1 Allele in African Populations Causes RBC Dehydration and Attenuates Plasmodium Infection. *Cell* **2018**, *173*, 443-455.e12, doi:10.1016/j.cell.2018.02.047.
46. Shmukler, B.E.; Vandorpe, D.H.; Rivera, A.; Auerbach, M.; Brugnara, C.; Alper, S.L. Dehydrated Stomatocytic Anemia Due to the Heterozygous Mutation R2456H in the Mechanosensitive Cation Channel PIEZO1: A Case Report. *Blood Cells, Molecules, and Diseases* **2014**, *52*, 53–54, doi:10.1016/j.bcmd.2013.07.015.
47. Andolfo, I.; Russo, R.; Rosato, B.E.; Manna, F.; Gambale, A.; Brugnara, C.; Iolascon, A. Genotype-Phenotype Correlation and Risk Stratification in a Cohort of 123 Hereditary Stomatocytosis Patients. *Am J Hematol* **2018**, *93*, 1509–1517, doi:10.1002/ajh.25276.
48. Rotordam, G.M.; Fermo, E.; Becker, N.; Barcellini, W.; Brüggemann, A.; Fertig, N.; Egée, S.; Rapedius, M.; Bianchi, P.; Kaestner, L. A Novel Gain-of-Function Mutation of Piezo1 Is Functionally Affirmed in Red Blood Cells by High-Throughput Patch Clamp. *Haematologica* **2019**, doi:10.3324/haematol.2018.201160.
49. Kaestner, L.; Christophersen, P.; Bernhardt, I.; Bennekou, P. The Non-Selective Voltage-Activated Cation Channel in the Human Red Blood Cell Membrane: Reconciliation between Two Conflicting Reports and Further Characterisation. *Bioelectrochemistry* **2000**, *52*, 117–125, doi:10.1016/s0302-4598(00)00110-0.
50. Kaestner, L.; Egée, S. Commentary: Voltage Gating of Mechanosensitive PIEZO Channels. *Frontiers in Physiology* **2018**, *9*, 1565, doi:10.3389/fphys.2018.01565.
51. Bouyer, G.; Cueff, A.; Egée, S.; Kmiecik, J.; Maksimova, Y.; Glogowska, E.; Gallagher, P.G.; Thomas, S.L.Y. Erythrocyte Peripheral Type Benzodiazepine Receptor/Voltage-Dependent Anion Channels Are Upregulated by Plasmodium Falciparum. *Blood* **2011**, *118*, 2305–2312, doi:10.1182/blood-2011-01-329300.
52. Mayer, K.D.; Starkey, B.J. Simpler Flame Photometric Determination of Erythrocyte Sodium and Potassium: The Reference Range for Apparently Healthy Adults. *Clin. Chem.* **1977**, *23*, 275–278, doi:10.1093/clinchem/23.2.275.
53. Baunbaek, M.; Bennekou, P. Evidence for a Random Entry of Ca2+ into Human Red Cells. *Bioelectrochemistry* **2008**, *73*, 145–150, doi:10.1016/j.bioelechem.2008.04.006.
54. Shmukler, B.E.; Rivera, A.; Bhargava, P.; Nishimura, K.; Hsu, A.; Kim, E.H.; Trudel, M.; Rust, M.B.; Hubner, C.A.; Brugnara, C.; et al. Combined Genetic Disruption of K-Cl Cotransporters and Gardos Channel KCNN4 Rescues Erythrocyte Dehydration in the SAD Mouse Model of Sickle Cell Disease. *Blood Cells, Mol., Dis.* **2019**, *79*, 102346, doi:10.1016/j.bcmd.2019.102346.
55. Philp, A.R.; Riquelme, T.T.; Millar-Büchner, P.; González, R.; Sepúlveda, F.V.; Cid, L.P.; Flores, C.A. Kcnn4 Is a Modifier Gene of Intestinal Cystic Fibrosis Preventing Lethality in the Cftr-F508del Mouse. *Sci. Rep.* **2018**, *8*, 9320, doi:10.1038/s41598-018-27465-3.

56. Yang, L.; Andrews, D.A.; Low, P.S. Lysophosphatidic Acid Opens a Ca++ Channel in Human Erythrocytes. *Blood* **2000**, *95*, 2420–2425, doi:10.1182/blood.v95.7.2420.007k12_2420_2425.
57. Wagner-Britz, L.; Wang, J.; Kaestner, L.; Bernhardt, I. Protein Kinase Ca and P-Type Ca 2+ Channel Ca V 2.1 in Red Blood Cell Calcium Signalling. *Cell Physiol Biochem* **2013**, *31*, 883–891, doi:10.1159/000350106.
58. Wang, J.; Hertz, L.; Ruppenthal, S.; Nemer, W.E.; Connes, P.; Goede, J.S.; Bogdanova, A.; Birnbaumer, L.; Kaestner, L. Lysophosphatidic Acid-Activated Calcium Signaling Is Elevated in Red Cells from Sickle Cell Disease Patients. *Cells* **2021**, *10*, 456, doi:10.3390/cells10020456.
59. Chu, X.; Tong, Q.; Cheung, J.Y.; Wozney, J.; Conrad, K.; Mazack, V.; Zhang, W.; Stahl, R.; Barber, D.L.; Miller, B.A. Interaction of TRPC2 and TRPC6 in Erythropoietin Modulation of Calcium Influx. *J Biol Chem* **2004**, *279*, 10514–10522, doi:10.1074/jbc.m308478200.
60. Foller, M.; Kasinathan, R.S.; Koka, S.; Lang, C.; Shumilina, E.V.; Birnbaumer, L.; Lang, F.; Huber, S.M. TRPC6 Contributes to the Ca(2+) Leak of Human Erythrocytes. *Cell Physiol Biochem* **2008**, *21*, 183–192.
61. Kaestner, L.; Minetti, G. The Potential of Erythrocytes as Cellular Aging Models. *Cell Death Differ* **2017**, *24*, 1475–1477, doi:10.1038/cdd.2017.100.
62. Klein, M.; Kaestner, L.; Bogdanova, A.Y.; Minetti, G.; Rudloff, S.; Lundby, C.; Makhro, A.; Seiler, E.; Cromvoirt, A.; Fenk, S.; et al. Absence of Neocytolysis in Humans Returning from a 3-week High-altitude Sojourn. *Acta Physiol* **2021**, *232*, e13647, doi:10.1111/apha.13647.
63. Makhro, A.; Hanggi, P.; Goede, J.S.; Wang, J.; Brüggemann, A.; Gassmann, M.; Schmugge, M.; Kaestner, L.; Speer, O.; Bogdanova, A. N-Methyl D-Aspartate (NMDA) Receptors in Human Erythroid Precursor Cells and in Circulating Red Blood Cells Contribute to the Intracellular Calcium Regulation. *AJP: Cell Physiology* **2013**, doi:10.1152/ajpcell.00031.2013.
64. Kucherenko, Y.V.; Wagner-Britz, L.; Bernhardt, I.; Lang, F. Effect of Chloride Channel Inhibitors on Cytosolic Ca2+ Levels and Ca2+-Activated K+ (Gardos) Channel Activity in Human Red Blood Cells. *J Membr Biol* **2013**, *246*, 315–326, doi:10.1007/s00232-013-9532-0.
65. Lin, Y.-C.; Guo, Y.R.; Miyagi, A.; Levring, J.; MacKinnon, R.; Scheuring, S. Force-Induced Conformational Changes in PIEZO1. *Nature* **2019**, *573*, 230–234, doi:10.1038/s41586-019-1499-2.
66. Kaestner, L.; Bogdanova, A.; Egee, S. Calcium Channels and Calcium-Regulated Channels in Human Red Blood Cells. *Adv Exp Med Biol* **2020**, *1131*, 625–648, doi:10.1007/978-3-030-12457-1_25.
67. Kaestner, L.; Wang, X.; Hertz, L.; Bernhardt, I. Voltage-Activated Ion Channels in Non-Excitable Cells-A Viewpoint Regarding Their Physiological Justification. *Front Physiol* **2018**, *9*, 450, doi:10.3389/fphys.2018.00450.
68. Gallagher, P.G. Disorders of Red Cell Volume Regulation. *Curr Opin Hematol* **2013**, *20*, 201–207, doi:10.1097/moh.0b013e32835f6870.
69. Fuchs, C.; Paschen, K.; Spieckermann, P.G.; Westberg, C. v. Bestimmung Des Ionisierten Calciums Im Serum Mit Einer Ionenselektiven Durchflußelektrode: Methodik Und Normalwerte. *Klin. Wochenschr.* **1972**, *50*, 824–832, doi:10.1007/bf01496340.
70. Liappis, N. [Sodium-, Potassium- and Chloride-Concentrations in the Serum of Infants, Children and Adults]. *Monatsschrift Fur Kinderheilkunde* **1972**, *120*, 138–142.
71. Schoeppe, W.; Brecht, H.M. [Frequency of Decreased and Increased Potassium Concentration in Plasma and Erythrocytes]. *Med. Klin.* **1969**, *64*, 736–739.
72. Tiffert, T.; Bookchin, R.M.; Lew, V.L. Calcium Homeostasis in Normal and Abnormal Human Red Cells. In; Bernhardt, I., Ellory, C., Eds.; Red Cell Membrane Transport in Health and Disease; 2003; pp. 373–405.
73. Smith, E.K. Observations on the Measurement and Regulation of the Sodium Content of Human Erythrocytes. *Clin. Sci.* **1972**, *42*, 447–453, doi:10.1042/cs0420447.
74. Rizzuto, V.; Mencattini, A.; Álvarez-González, B.; Giuseppe, D.D.; Martinelli, E.; Beneitez-Pastor, D.; Mañú-Pereira, M. del M.; Lopez-Martinez, M.J.; Samitier, J. Combining Microfluidics with Machine Learning Algorithms for RBC Classification in Rare Hereditary Hemolytic Anemia. *Sci Rep-uk* **2021**, *11*, 13553, doi:10.1038/s41598-021-92747-2.
75. Egee, S.; Kaestner, L. The Transient Receptor Potential Vanilloid Type 2 (TRPV2) Channel - a New Druggable Ca2+ Pathway in Red Cells, Implications for Red Cell Ion Homeostasis. *Frontiers in Physiology* **2021**, *12*, 677573, doi:10.3389/fphys.2021.677573.
76. Belkacemi, A.; Fecher-Trost, C.; Tinschert, R.; Flormann, D.; Malihpour, M.; Wagner, C.; Meyer, M.R.; Beck, A.; Flockerzi, V. The TRPV2 Channel Mediates Ca2+ Influx and the Δ9-THC-Dependent Decrease in Osmotic Fragility in Red Blood Cells. *Haematologica* **2021**, *106*, 2246–2250, doi:10.3324/haematol.2020.274951.
77. Chari-Bitron, A.; Shahar, A. Changes in Rat Erythrocyte Membrane Induced ByΔ1-Tetrahydrocannabinol, Scanning Electron Microscope Study. *Experientia* **1979**, *35*, 365–366, doi:10.1007/bf01964355.
78. Flormann, D.; Qiao, M.; Murciano, N.; Iacono, G.; Darras, A.; Hof, S.; Recktenwald, S.M.; Rotordam, M.G.; Becker, N.; Geisel, J.; et al. Transient Receptor Potential Channel Vanilloid Type 2 in Red Cells of Cannabis Consumer. *Am. J. Hematol.* **2022**, *97*, E180–E183, doi:10.1002/ajh.26509.

79. Beutler, E. Biphasic Loss of Red Cell Enzyme Activity during in Vivo Aging. *Prog. Clin. Biol. Res.* **1985**, *195*, 317–333.
80. Chasis, J.A.; Prenant, M.; Leung, A.; Mohandas, N. Membrane Assembly and Remodeling during Reticulocyte Maturation. *Blood* **1989**, *74*, 1112–1120.
81. Tiffert, T.; Daw, N.; Etzion, Z.; Bookchin, R.M.; Lew, V.L. Age Decline in the Activity of the Ca2+-Sensitive K+ Channel of Human Red Blood Cells. *J. Gen. Physiol.* **2007**, *129*, 429–436, doi:10.1085/jgp.200709766.
82. Vasileva, V.; Chubinskiy-Nadezhdin, V. Regulation of PIEZO1 Channels by Lipids and the Structural Components of Extracellular Matrix/Cell Cytoskeleton. *J. Cell. Physiol.* **2023**, *238*, 918–930, doi:10.1002/jcp.31001.
83. Lin, Y.; Buyan, A.; Corry, B. Computational Studies of Piezo1 Yield Insights into Key Lipid–Protein Interactions, Channel Activation, and Agonist Binding. *Biophys. Rev.* **2022**, *14*, 209–219, doi:10.1007/s12551-021-00847-0.
84. Buyan, A.; Cox, C.D.; Barnoud, J.; Martinac, B.; Marrink, S.-J.; Corry, B. Understanding Piezo1's Relationship with Lipids. *Biophys. J.* **2019**, *116*, 459a, doi:10.1016/j.bpj.2018.11.2481.
85. Minetti, G.; Kaestner, L.; Dorn, I. Terminal Maturation of Human Reticulocytes to Red Blood Cells by Extensive Remodelling and Progressive Liquid Ordering of Membrane Lipids. **2023**, doi:10.1101/2023.06.02.543386.
86. Beutler, E.; West, C.; Blume, K.G. The Removal of Leukocytes and Platelets from Whole Blood. *J Laboratory Clin Medicine* **1976**, *88*, 328–333.
87. Achilli, C.; Ciana, A.; Balduini, C.; Risso, A.; Minetti, G. Application of Gelatin Zymography for Evaluating Low Levels of Contaminating Neutrophils in Red Blood Cell Samples. *Anal Biochem* **2011**, *409*, 296–297, doi:10.1016/j.ab.2010.10.019.
88. Tyanova, S.; Temu, T.; Cox, J. The MaxQuant Computational Platform for Mass Spectrometry-Based Shotgun Proteomics. *Nat. Protoc.* **2016**, *11*, 2301–2319, doi:10.1038/nprot.2016.136.
89. Huber, W.; Carey, V.J.; Gentleman, R.; Anders, S.; Carlson, M.; Carvalho, B.S.; Bravo, H.C.; Davis, S.; Gatto, L.; Girke, T.; et al. Orchestrating High-Throughput Genomic Analysis with Bioconductor. *Nat. Methods* **2015**, *12*, 115–121, doi:10.1038/nmeth.3252.
90. Vizcaíno, J.A.; Deutsch, E.W.; Wang, R.; Csordas, A.; Reisinger, F.; Ríos, D.; Dianes, J.A.; Sun, Z.; Farrah, T.; Bandeira, N.; et al. ProteomeXchange Provides Globally Coordinated Proteomics Data Submission and Dissemination. *Nat. Biotechnol.* **2014**, *32*, 223–226, doi:10.1038/nbt.2839.
91. Heshusius, S.; Heideveld, E.; Burger, P.; Thiel-Valkhof, M.; Sellink, E.; Varga, E.; Ovchynnikova, E.; Visser, A.; Martens, J.H.A.; Lindern, M. von; et al. Large-Scale in Vitro Production of Red Blood Cells from Human Peripheral Blood Mononuclear Cells. *Blood Adv* **2019**, *3*, 3337–3350, doi:10.1182/bloodadvances.2019000689.
92. Macey, R.I.; Adorante, J.S.; Orme, F.W. Erythrocyte Membrane Potentials Determined by Hydrogen Ion Distribution. *Biochimica Et Biophysica Acta Bba - Biomembr* **1978**, *512*, 284–295, doi:10.1016/0005-2736(78)90253-5.
93. Ma, S.; Qi, X.; Han, K.; Wang, S.; Hu, G.; Li, X. Computational Investigation of Flow Dynamics and Mechanical Retention of Age-Associated Red Blood Cells in the Spleen. *Phys. Rev. Fluids* **2023**, *8*, 063103, doi:10.1103/physrevfluids.8.063103.
94. Nardo-Marino, A.; Glenthøj, A.; Brewin, J.N.; Petersen, J.; Braunstein, T.H.; Kurtzhals, J.A.L.; Williams, T.N.; Rees, D.C. Decreased Red Blood Cell Deformability Contributes to Loss of Splenic Filtration Function and Variations in Spleen Size in Children with Sickle Cell Anaemia. *Blood* **2022**, *140*, 1639–1640, doi:10.1182/blood-2022-165460.
95. Kaestner, L.; Bernhardt, I. Further Characterisation of the Non-Selective Cation Channel in the Human Red Blood Cell Membrane.; 2001; p. 9.
96. Steffen, P.; Jung, A.; Nguyen, D.B.; Müller, T.; Bernhardt, I.; Kaestner, L.; Wagner, C. Stimulation of Human Red Blood Cells Leads to Ca2+-Mediated Intercellular Adhesion. *Cell Calcium* **2011**, *50*, 54–61, doi:10.1016/j.ceca.2011.05.002.